THE JOURNAL OF PHYSICAL CHEMISTRY C

Article

Cite This: J. Phys. Chem. C 2019, 123, 18180−18186

pubs.acs.org/JPCC

Understanding the Decomposition Mechanisms of $LiNH_2$, $Mg(NH_2)_2$, and $NaNH_2$: A Joint Experimental and Theoretical Study

Huai-Jun Lin,*[,†] Peng Zhang,[†] Yan-Xiong Fang,[‡] Yu-Jun Zhao,[§] Haichang Zhong,[∥] and Jia-Jun Tang*[,‡,§]

[†]Institute of Advanced Wear & Corrosion Resistance and Functional Materials, Jinan University, Guangzhou 510632, China

[‡]Institute of Natural Medicine and Green Chemistry, School of Chemical Engineering and Light Industry, Guangdong University of Technology, Guangzhou 510006, China

[§]Department of Physics, South China University of Technology, Guangzhou 510640, China

[∥]School of Materials Science and Engineering, Fujian Provincial Key Laboratory of Functional Materials and Applications, Xiamen University of Technology, Xiamen 361024, China

ABSTRACT: Metal amides are promising candidates for hydrogen storage, hydrogen production, NH_3 synthesis and cracking, and so on. However, the decomposition behaviors and mechanisms of metal amides remain unclear. In this study, the decomposition properties of three metal amides, including $LiNH_2$, $Mg(NH_2)_2$, and $NaNH_2$, are studied by thermogravimetry, mass spectroscopy, and in situ X-ray diffraction techniques combined with density functional theory (DFT) calculations. It is found that $Mg(NH_2)_2$, $LiNH_2$, and $NaNH_2$ exhibit very different metal−N and N−H bond strengths, which precipitate various formations energies of different kinds of vacancies. As a result, $LiNH_2$ releases a major amount of NH_3, with a small amount of N_2 at a temperature as high as 350 °C. $Mg(NH_2)_2$ releases NH_3 and N_2 synchronously at a temperature range of 300−400 °C without the emission of H_2. $NaNH_2$ synchronously releases H_2, NH_3, and a small amount of N_2, at a narrow temperature range of 275−290 °C. Using DFT calculations, the decomposition behaviors and the corresponding decomposition mechanisms for $LiNH_2$, $Mg(NH_2)_2$, and $NaNH_2$ have been well understood.

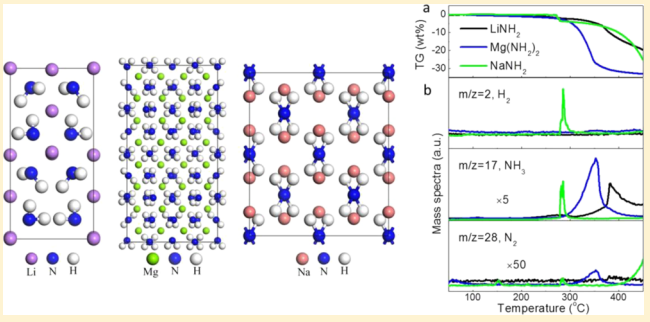

1. INTRODUCTION

Metal amides, for example, $LiNH_2$ and $NaNH_2$, have been synthesized more than a century ago.[1] They have been widely used as reagents in organic synthesis for industrial productions. Since 2002, metal amides have been tremendously studied as hydrogen storage materials.[2−5] By thoroughly mixing them with metal hydrides to form composites, such as $LiNH_2$−LiH,[6,7] $Mg(NH_2)_2$−LiH,[8−10] $LiNH_2$−MgH_2,[11] $Mg(NH_2)_2$−MgH_2,[12−14] and many others,[4,15−20] promising hydrogen storage properties could be achieved, including hydrogen storage capacity above 5 wt %, reversible hydrogenation/dehydrogenation, and moderate thermodynamics. The $LiNH_2$−LiH composite with good hydrogen storage reversibility was first reported by Chen[6] et al., following reaction 1 to store ∼7 wt % of hydrogen:

$$LiNH_2 + LiH = Li_2NH + H_2 \quad (1)$$

Although the redox reaction between $H^{\delta+}$ in amides and $H^{\delta-}$ in hydrides was suggested by Xiong[8] et al. to be the key for the outstanding hydrogen desorption properties of amide-hydride composites, it was also proposed by Ichikawa[21] et al. that the reaction 1 was consisted of two elementary solid−gas reactions mediated by ammonia (NH_3)

$$2LiNH_2 = Li_2NH + NH_3 \quad (2)$$

$$LiH + NH_3 = LiNH_2 + H_2 \quad (3)$$

Therefore, more or less NH_3 could be detected during the decomposition of $LiNH_2$-based composites.[22] Besides being considered as promising candidates for hydrogen storage, metal amides also attract much interest in the field of hydrogen production[23] and NH_3 cracking[24,25] and synthesis.[26] David[23] et al. reported the role of $NaNH_2$ for NH_3 cracking following two reactions:

$$NaNH_2 \rightarrow Na + 1/2N_2 + H_2 \quad (4)$$

$$Na + NH_3 \rightarrow NaNH_2 + 1/2H_2 \quad (5)$$

leading to a neat reaction: $2NH_3(g) \xrightarrow{Na + NaNH_2} N_2(g) + H_2(g)$. The $Na/NaNH_2$ system shows superior performance to supported nickel and ruthenium catalysts, reaching 99.2% decomposition efficiency with 0.5 g of $NaNH_2$ in a 60 sccm NH_3 flow at 530 °C. Wang[26]

Received: April 14, 2019
Revised: July 11, 2019
Published: July 12, 2019

DOI: 10.1021/acs.jpcc.9b03524
J. Phys. Chem. C 2019, 123, 18180−18186

et al. reported a novel two-active-center catalysis, that is, TM-mediated (TM = transition metal) with LiH, to create an energy-efficient pathway that allows NH_3 synthesis under mild conditions. The NH_3 synthesis process is through nitrogen transfer and hydrogenation and can be briefly described as follows:

$$N_2 + 2^* = 2N^* \quad (6)$$

$$N^* + LiH^* \rightarrow [LiNH] \quad (7)$$

$$[LiNH] + H_2 \rightarrow LiH + NH_3 \quad (8)$$

where * represents a metal-surface site, and $LiNH_2$ and Li_2NH are collectively denoted as [LiNH].

Except for $NaNH_2$, NH_3 was usually considered as the only gaseous decomposition product for metal amides.[22,27,28] Song[28] and Yang reported a decomposition mechanism of $Mg(NH_2)_2$ based on the bonding characteristics. The proposed decomposition of the $Mg(NH_2)_2$ is consisted of two steps: (1) H^+ cations decompose from the $[NH_2]$ ligands, and then $[NH_2]^-$ anions decompose. The H^+ cations and $[NH_2]^-$ anions therefore react with each other to generate NH_3. Nevertheless, N_2 was also noted as a possible gaseous product for decompositions of metal amides. Cao[29] et al. reported that the gaseous decomposition products of $Rb_2[Mn(NH_2)_4]$ contained N_2, H_2, and NH_3. The decomposition of metal amides is an important issue for their hydrogen storage, hydrogen production, and NH_3 cracking and synthesis properties; however, there remains controversy and unclearness on their decomposition behaviors. Therefore, the decomposition of metal amides should be comprehensively restudied.

In this study, the decomposition properties of three metal amides, including $LiNH_2$, $Mg(NH_2)_2$, and $NaNH_2$, are studied by thermogravimetry−mass spectroscopy (TG−MS) and in situ X-ray diffraction (XRD) experiments combined with density functional theory (DFT) calculations. It shows that the decompositions of these metal amides are very different from each other due to the different metal−N and N−H bond strengths for the amides. Using TG−MS and in situ XRD combined with DFT calculations, the decomposition behaviors and the corresponding decomposition mechanisms for $LiNH_2$, $Mg(NH_2)_2$, and $NaNH_2$ could be well understood.

2. EXPERIMENTAL AND COMPUTATIONAL DETAILS

2.1. Materials and Experimental Methods. The starting powder samples were $LiNH_2$ (98% purity, Aldrich), $Mg(NH_2)_2$ (95% purity, DICP, China), and $NaNH_2$ (95% purity, Aldrich). The dehydrogenation properties were studied by TG using an NETZSCH 449 thermal analyzer, and a mass spectroscopy (MS) system (Hiden-Qic 20) was attached with the TG system to simultaneously monitor the evolved gas species. Samples of about 10 mg were taken in an Al_2O_3 pan and heated under an Ar atmosphere (100 mL min^{-1}) from room temperature to 450 °C under a consistent heating rate of 5 K min^{-1}. The TG−MS machine was placed in an Ar-protected glovebox to avoid oxidation or hydrolysis during the whole experiment period. In situ decomposition XRD experiments were performed in a Rigaku XRD machine under a pressure of around 3×10^{-3} MPa.

2.2. Computational Methods. Periodic spin-polarized DFT calculations are performed using the Vienna Ab initio Simulation Package.[30−32] The Perdew−Burke−Ernzerhof functional is used to account for electron exchange−correlation effects,[33] and the projector-augmented wave method is used to approximate core electrons.[34] The plane-wave cutoff energy is set to be 450 eV. For Li, Na, Mg, N, and H species, their respective (1s), (2s), (2s), (2s, 2p), and (1s) states are treated as valence electrons.

For calculations of $LiNH_2$, $NaNH_2$, and $Mg(NH_2)_2$ bulks with and without various types of vacancies, integrations over the first Brillouin zone are performed using the Monkhorst−Pack *k*-point sampling method with Γ-centered 4 × 4 × 2, 4 × 3 × 4, and 4 × 4 × 2 grids,[35] where adequate *k*-point mesh tests are carried out. It results in total energies converging to a precision of ∼1 meV per unit cell. For the defect-free bulk optimizations, both the atom and the cell are allowed to relax. For the vacancy calculations, atoms in the unit cell are allowed to relax while the unit cell is fixed at the bulk value. The optimizations are done until forces on the atoms are less than 0.02 eV $Å^{-1}$ and the total energy change between two successive steps is less than 1×10^{-5} eV.

We consider the formation energies of various vacancy types, including V_N, V_H, V_{NH}. V_{NH_2}, and V_{NH_3}. The formula to calculate the formation energy of various types of vacancy is as follows:

$$E_{\text{formation}}^{(\alpha,q)} = E(\alpha, q) - E(0) + \sum_{\alpha} n_\alpha \mu_\alpha + q(E_{\text{VBM}} + E_{\text{F}}) \quad (9)$$

where $E(\alpha,q)$ and $E(0)$ are the total energy of the unit cell with and without defect α, μ_α is the absolute value of the chemical potential of atom α, n_α is the number of defect atoms, q is the charge state, and E_{VBM} and E_{F} are the energy of valence band maximum and the Fermi energy, respectively. In our cases, we consider the charge neutral defects ($q = 0$).

We choose the lattices as our calculation mediums based on two considerations: first, the bulk calculations have been widely seen in the thermodynamic calculations of decomposition in $LiNH_2$ and Li_2NH,[36] $Mg(NH_2)_2$,[28] $Mg(BH_4)_2 \cdot 2NH_3$, and $LiMg(BH_4)_2 \cdot 2NH_3$[37] as well as the kinetics calculation of H vacancy diffusions in MgH_2,[38] indicating that bulk calculations can be representative and qualitatively indicative. Second, the adoption of various metal amide surfaces involves choice of surface miller index and surface termination, which could be difficult due to the current shortage of a systematic theoretical study on surface stabilities of these amides. We have found that the surface stabilities and terminations have a great influence on the surface or interfaces properties in the systems of Mg,[39,40] Mg/MgH_2,[41] and $CeH_{2.73}/CeO_2$.[42] Considering that the main goal of our study is to locate the commons in and differences between these metal amides, we choose bulk calculations as our main measure to investigate the mechanism of these metal amide decompositions. Importantly, we pay great attention on the possibility that leads to the release of N_2 that may have been neglected in the previous literature studies.

2.3. Lattices of $LiNH_2$, $Mg(NH_2)_2$, and $NaNH_2$. The calculated lattice constants of tetrahedral $LiNH_2$, orthorhombic $NaNH_2$, and tetragonal $Mg(NH_2)_2$ unit cells are listed in Table 1. They are all in good agreement with the experimental and theoretical values.

DOI: 10.1021/acs.jpcc.9b03524
J. Phys. Chem. C 2019, 123, 18180−18186

Table 1. Space Group and Calculated Lattice Constants of $Mg(NH_2)_2$, $LiNH_2$, and $NaNH_2$

	space group	calculated lattice constant (Å)	reference (Å)
$LiNH_2$	$I\bar{4}$	$a = b = 4.976$, $c = 10.297$	$a = b = 5.043$, $c = 10.226$[c]
			$a = b = 5.034$, $c = 10.255$[d]
$Mg(NH_2)_2$	$I4_1/acd$	$a = b = 10.368$, $c = 20.197$	$a = b = 10.376$, $c = 20.062$[a]
			$a = b = 10.445$, $c = 20.312$[b]
$NaNH_2$	$Fddd$	$a = 8.878$, $b = 10.384$, $c = 8.076$	$a = 8.949$, $b = 10.456$, $c = 8.061$[e]
			$a = 8.907$, $b = 10.726$, $c = 8.289$[f]

[a]Reference 45. [b]Reference 46. [c]Reference 47. [d]Reference 48. [e]Reference 43. [f]Reference 44.

3. RESULTS AND DISCUSSION

3.1. Decomposition of $LiNH_2$. Figure 1 shows the TG–MS profiles of $LiNH_2$. It could be clearly seen that there is a main release of NH_3 gas during the whole decomposition process, and a small amount of N_2 at a high temperature above 350 °C was observed. The mass loss of $LiNH_2$ heating to 450 °C is only 20 wt %, which is due to the incomplete desorption of $LiNH_2$. The TG–MS curves are similar to the results reported by Yao[49] et al., in which the desorption is almost completed by heating to around 600 °C. The decomposition process is further studied by in situ XRD as shown in Figure 2. The decomposition of $LiNH_2$ from room temperature to 450 °C could be summarized as follows:

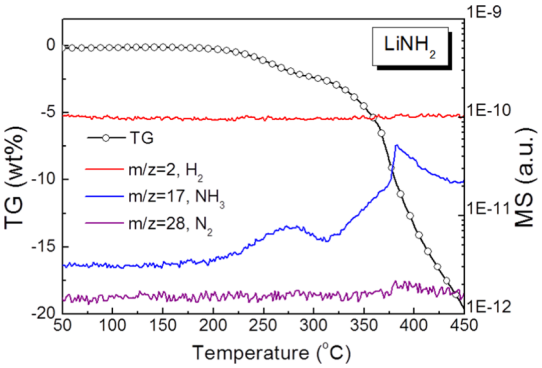

Figure 1. TG–MS profiles of $LiNH_2$, at a heating rate of 5 K min^{-1}.

$$2LiNH_2 \rightarrow (Li_{1+x}NH_{2-x} + NH_3 \rightarrow Li_{1+y}NH_{2-y} + NH_3 \rightarrow Li_{1+z}NH_{2-z} + NH_3) \rightarrow Li_2NH + NH_3 \quad (0 \le x < y < z \le 1) \quad (10)$$

To understand the decomposition process, formation energies (E_f) of various types of vacancies in $LiNH_2$, whose structure is shown in Figure 3, are calculated and listed in Table 2. We can see that V_H is the most energetically favored single vacancy with formation energies of 2.39 and 2.38 eV, respectively. However, the formation energy of V_{NH_3} is only 2.00 eV, which is 0.39 eV lower than that of V_H. The NH_3 formation energy preference is unique among the three metal amide systems studied in the present work, and it is congruent with our experimental observation that NH_3 is the main product (Figure 1). With the formation of NH_3-vacancy, the formation energy of N-vacancy is greatly reduced in $LiNH_2$, which means that the release of N_2 gas at temperature high enough is possible.

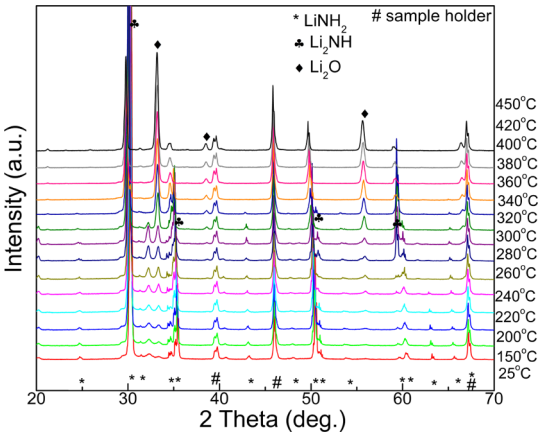

Figure 2. In situ decomposition XRD patterns of $LiNH_2$, as a heating rate of 10 K min^{-1}.

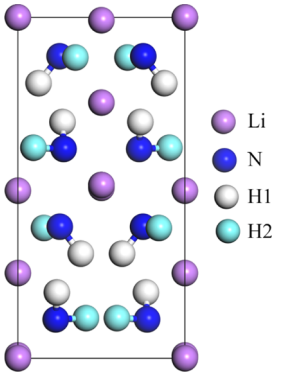

Figure 3. Side view of the $LiNH_2$ unit cell.

Table 2. Formation Energies of Various Types of Vacancies in Pure and Defected $LiNH_2$[a]

unit cell	vacancy type	E_f (eV)	description
$LiNH_2$	V_N	6.28	N
	V_{H1}	2.39	H1
	V_{H2}	2.39	H2
	$2V_H$	4.48	H1 + H2
	V_{NH_2}	4.26	NH_2
	V_{NH_3}	2.00	NH_2 + H1
	V_{NH_3}	2.06	NH_2 + H2
V_{H1}–$LiNH_2$	V_{NH_2}	2.23	NH_2
	V_{H1}	2.10	H2
	V_{N1}	2.19	N
	V_{NH}	3.92	N, H2
$2V_{H1}$–$LiNH_2$	V_N	1.35	N

[a]The parenthesis in the column of description denotes the location of the vacancies. In $LiNH_2$, there are two types of H atoms, H1 and H2, bonded to the same N forming an amidogen radical.

3.2. Decomposition of $Mg(NH_2)_2$. The decomposition products of $Mg(NH_2)_2$ and $LiNH_2$ were usually considered as NH_3 and the corresponding imides/nitrides, excluding N_2. However, TG–MS study indicates that N_2 is also a main decomposition product of $Mg(NH_2)_2$. As shown in Figure 4,

DOI: 10.1021/acs.jpcc.9b03524
J. Phys. Chem. C 2019, 123, 18180–18186

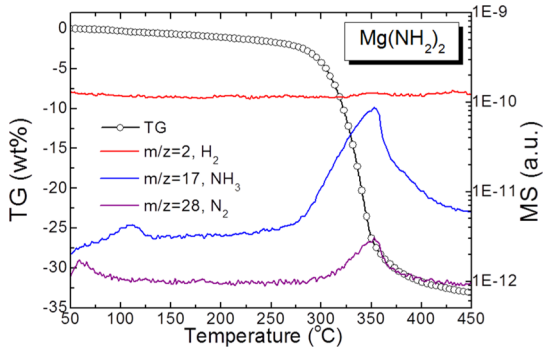

Figure 4. TG−MS profiles of $Mg(NH_2)_2$, at a heating rate of 5 K min^{-1}.

there is a synchronous release of NH_3 and N_2 without H_2 emission at the temperature range of 300−400 °C. The release of N_2 is very unique in the decomposition process of $Mg(NH_2)_2$ and should be further studied.

We first consider different single vacancy cases for V_N and V_H (see Figure 5). Table 3 shows the formation energies of

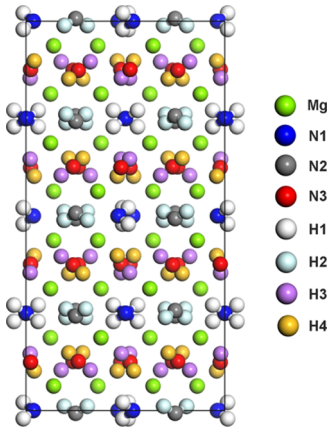

Figure 5. Side view of the $Mg(NH_2)_2$ unit cell.

various vacancies. The formation energies of V_{N1}, V_{N2}, and V_{N3} are 6.84, 7.16, and 6.65 eV, respectively, while the ones of V_{H1}, V_{H2}, V_{H3}, and V_{H4} are 2.67, 2.71, 2.7, and 2.7 eV, respectively. It can be seen that the H vacancy formation is much more energetically favored than the N vacancy ones. Then, the formation of group vacancy is considered. In the $Mg(NH_2)_2$ bulk, each N atom is bonded to two H atoms and forms an amidogen radical, NH_2. It is found that the formation energies of V_{NH}, V_{NH_2}, and V_{NH_3} are found to be 5.55, 4.73, and 3.5 eV. The above-mentioned NH_3 vacancy is the combination of the N3 amidogen radical and the H atom bonded to N1. Among these three types of group vacancies, the NH_3 vacancy formation is the most energetically favored.

In Table 3, we also notice that, in V_{H1}−$Mg(NH_2)_2$, the formations of V_H and V_N are most energetically preferred with formation energies of 2.13 and 2.41 eV. The H deprivation from an NH_2 group in pristine $Mg(NH_2)_2$ greatly destroys the strong N−H hybridizations[28] and thus conspicuously lowers the V_N formation energy to 2.41 eV, which is merely 0.28 eV higher than the V_H one of 2.13 eV in V_{H1}−$Mg(NH_2)_2$. It means that the concurrent formation of V_N and V_H is possible in V_{H1}−$Mg(NH_2)_2$, which could lead to the formation of NH_3. Moreover, the dramatic difference between the V_H, V_N

Table 3. Formation Energies of Various Types of Vacancies in Pure and Defected $Mg(NH_2)_2$[a]

unit cell	vacancy type	E_f (eV)	description
$Mg(NH_2)_2$	V_{N1}	6.84	N1
	V_{N2}	7.16	N2
	V_{N3}	6.65	N3
	V_{H1}	2.67	H1(N1)
	V_{H2}	2.71	H2(N2)
	V_{H3}	2.70	H3(N3)
	V_{H4}	2.70	H4(N3)
	$2V_H$	4.80	H1(N1)
	V_{NH}	5.55	NH(N3)
	V_{NH_2}	4.73	NH_2(N1)
	V_{NH_2}	4.87	NH_2(N2)
	V_{NH_2}	4.84	NH_2(N3)
	V_{NH_3}	3.73	NH_2(N1) + H(N2)
	V_{NH_3}	3.73	NH_2(N1) + H(N3)
	V_{NH_3}	3.54	NH_2(N2) + H(N1)
	V_{NH_3}	3.82	NH_2(N2) + H(N3)
	V_{NH3}	3.50	NH_2(N3) + H(N1)
	V_{NH_3}	3.80	NH_2(N3) + H(N2)
	V_{NH_3}	3.61	NH_2(N3) + H(N3)
V_{H1}−$Mg(NH_2)_2$	V_{NH_2}	3.48	NH_2(N2)
	V_{NH_2}	3.45	NH_2(N3)
	V_{H1}	2.13	H1(N1)
	V_{N1}	2.41	N1
	V_{NH}	4.11	N1,H1(N1)
$2V_{H1}$−$Mg(NH_2)_2$	V_N	1.50	N(N2)
V_{NH_3}−$Mg(NH_2)_2$	V_{H1}	2.38	H1(N1)
	V_{N1}	0.48	N1

[a]The parenthesis in the column of description denotes the location of the vacancies.

formation energies, and the V_{NH} one (i.e., 4.11 eV) is larger than 1 eV. It implies that the formation of an NH_3 molecule is in consecutive separate steps of single V and H vacancy formations. In detail, the consecutive steps are as follows: the first single V_H, the second single V_H, the single V_N, and the single V_H. Then, an NH_3 molecule forms.

Interestingly, various n_N to n_H ratios in NH_3 (i.e., 1:3) and $Mg(NH_2)_2$ (i.e., 1:2) could result in, after major NH_3 formation, a plethora of N atoms, and thus, a trivial amount of N_2 formed. Table 3 shows that, in V_{NH_3}−$Mg(NH_2)_2$, the V_N formation energy of 0.48 eV is 1.9 eV lower than the V_H one of 2.38 eV, indicating that, after release of NH_3, the single N vacancy formation is very possible. It could lead to the formation of N_2 molecule. Our theoretical results are in qualitative agreement with our experimental NH_3 and N_2 observations (Figure 4), as well as the previous report where NH_3 is the main detected gas product.[8]

3.3. Decomposition of $NaNH_2$: Comparisons of Vacancy Formation and Calculation Limitation. The decomposition reaction of $NaNH_2$ was first reported by Titherley in 1894,[1] which consists of two steps as follows

$$NaNH_2 \rightarrow Na + 1/2N_2 + H_2 \quad (11)$$

$$NaNH_2 \rightarrow NaH + 1/2N_2 + 0.5H_2 \quad (12)$$

The presence of NaH or Na as final product depends on the back pressure of the system. Jain[17] et al. recently reported that

DOI: 10.1021/acs.jpcc.9b03524
J. Phys. Chem. C 2019, 123, 18180−18186

$NaNH_2$ decomposes directly into Na and NH_3 as major products with a small amount of N_2 and H_2. Figure 6 shows

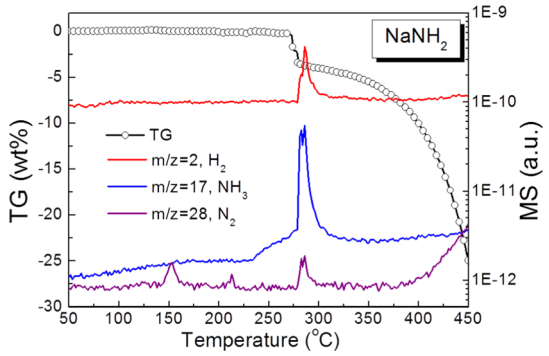

Figure 6. TG−MS profiles of $NaNH_2$ at a heating rate of 5 K min^{-1}.

the TG−MS profiles of $NaNH_2$. It is very unique that NH_3 and H_2 are the main decomposition products, meanwhile a small amount of N_2 was observed. In order to understand the decomposition mechanism, formation energies, E_f, of various types of vacancies in $NaNH_2$ are calculated and listed in Table 4.

Table 4. Formation Energies of Various Types of Vacancies in Pure and Defected $NaNH_2$[a]

unit cell	vacancy type	E_f (eV)	description
$NaNH_2$	V_N	5.60	N
	V_H	2.38	H
	$2V_H$	4.48	H + H
	V_{NH_2}	3.68	NH_2
	V_{NH_3}	2.69	NH_2 + H
V_H−$NaNH_2$	V_{NH_2}	2.93	NH_2
	V_H	2.10	H
	V_N	4.15	N
	V_{NH}	3.35	NH
$2V_H$−$NaNH_2$	V_N	0.78	N

[a]The parenthesis in the column of Description denotes the location of the vacancies. In $NaNH_2$, there is just one type of H.

The structure of $NaNH_2$ is shown in Figure 7. It is clear that V_H is the most energetically favored single vacancy with a formation energy of 2.38 eV. The V_N, V_H, and V_{NH_3} formation energies are 5.60, 2.38, and 2.69 eV, respectively. It manifests easy V_H and possible NH_3 formations. Very intriguingly, in V_H−$NaNH_2$, the V_H formation is the most energetically favored with a thermodynamic advantage of over 0.83 eV, compared to other possible vacancies. In this unique case, it is very likely for H_2 to form, which could be clearly seen from the MS spectra in Figure 6. The V_N formation is expedited by utter H depletion in the NH_2 group, with an E_f of only 0.78 eV, leading to the N_2 formation.

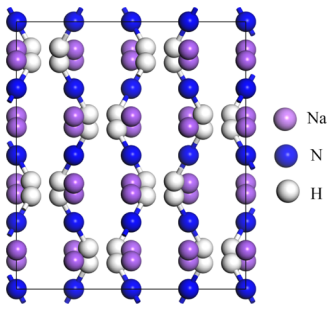

Figure 7. Side view of the $NaNH_2$ unit cell.

Based on our above thermodynamic results of vacancy formation, we find that these three metal amides share similar formation energies of single V_H from 2.38 to 2.67 eV and have difficulties of directly releasing N_2 from pure lattice (i.e., E_f of sing V_N is larger than 5.6 eV). In detail, $LiNH_2$, $Mg(NH_2)_2$, and $NaNH_2$ have formation energies of 2.38, 2.67, and 2.39 eV, respectively, indicating that $Mg(NH_2)_2$ has the strongest N−H bond among the three. However, $LiNH_2$ has a V_{NH_3} formation energy lower than its single V_H, implying a possibility of direct formation of NH_3 at room temperature and a late formation of N_2 at higher temperature. This lower formation energy of V_{NH_3} manifests that the metal−N bond is the weakest in $LiNH_2$. We assume that the late formation of N_2 at higher temperature is because the easy release of NH_3 takes place early and takes up H atoms 3 times as N atoms, leaving N atoms in the bulk. Different from $LiNH_2$, the two other metal amides, $Mg(NH_2)_2$ and $NaNH_2$, have a single V_H formation energy lower than V_{NH_3}. In these two metal amides, it is more likely to form NH_3 from consecutive steps (e.g., consecutive formations of V_H, V_H, V_N, and V_H). It implies that, in these two scenarios, the release of N_2 could take place at lower temperatures. By viewing the similarities and differences of these three metal amides, we infer that the vacancy formation mechanisms can be very different, thus causing experimental observations of different gas products at various temperatures.

We need to point out the limitation of this theoretical $NaNH_2$ solid models. Because the melting point of $NaNH_2$ is around 483 K, the decomposition of $NaNH_2$ to form NH_3, H_2, and N_2 takes place above 550 K. Because the focuses of our first-principles calculations are the similarities and differences between vacancy formations in these metal amides at 0 K, we deem that the calculations in $NaNH_2$ can still facilitate the viewing of a fuller decomposition picture.

4. SUMMARY

In this study, the decomposition properties of three metal amides including $LiNH_2$, $Mg(NH_2)_2$, and $NaNH_2$, are interpreted by TG−MS and in situ XRD experiments combined with DFT calculations. It is found in our DFT calculations that $Mg(NH_2)_2$, $LiNH_2$, and $NaNH_2$ exhibit different metal−N and N−H bond strengths, which lead to various formation energies of different kinds of vacancies, and various decomposition properties that are in qualitative agreement with our experimental observations. The three metal amides share similar formation energies of single V_H from 2.38 to 2.67 eV and have difficulties of directly releasing N_2 from pure lattice. $LiNH_2$ has a V_{NH_3} formation energy lower than its single V_H, implying a possibility of direct formation of NH_3 at low temperatures and a late formation of N_2 as temperature increases. $Mg(NH_2)_2$ and $NaNH_2$ have a single V_H formation energy lower than V_{NH_3}. In these two metal amides, it is more likely to form NH_3 from consecutive steps, and the release of N_2 could take place at lower temperatures. With TG−MS and DFT calculations, the decomposition behaviors and the corresponding decomposition mechanisms for $LiNH_2$, $Mg(NH_2)_2$, and $NaNH_2$ could be well understood.

DOI: 10.1021/acs.jpcc.9b03524
J. Phys. Chem. C 2019, 123, 18180−18186

AUTHOR INFORMATION

Corresponding Authors

*E-mail: hjlin@jnu.edu.cn (H.-J.L.).
*E-mail: pcntsfad@gmail.com (J.-J.T.).

ORCID

Huai-Jun Lin: 0000-0002-4505-9562
Yu-Jun Zhao: 0000-0002-6923-1099
Jia-Jun Tang: 0000-0002-0413-8862

Notes

The authors declare no competing financial interest.

ACKNOWLEDGMENTS

This study is supported by the open fund of Fujian Provincial Key Laboratory of Functional Materials and Applications (Xiamen University of Technology), the Fundamental Research Funds for the Central Universities (no. 21619415), and National Key R&D Program of China (2017YFB0305100) and Guangdong Science and Technology Plan Project "New Research & Development Organization—Guangdong Zhonghe Zhongde Fine Chemical Research and Development Co., Ltd." (2016B090934002).

REFERENCES

(1) Titherley, A. W. XLV.-Sodium, Potassium, and Lithium Amides. *J. Chem. Soc., Trans.* **1894**, *65*, 504−522.
(2) Paik, B.; Li, H.-W.; Wang, J.; Akiba, E. Composite as H_2 Storage Material: a Case Study with $Mg(NH_2)_2$-4LiH-$LiNH_2$. *Chem. Commun.* **2015**, *51*, 10018−10021.
(3) Li, H.-W.; Yan, Y.; Orimo, S.-i.; Züttel, A.; Jensen, C. M. Recent Progress in Metal Borohydrides for Hydrogen Storage. *Energies* **2011**, *4*, 185−214.
(4) Wang, J.; Li, H.-W.; Chen, P. Amides and Borohydrides for High-Capacity Solid-State Hydrogen Storage Materials Design and Kinetic Improvements. *MRS Bull.* **2013**, *38*, 480−487.
(5) Garroni, S.; Santoru, A.; Cao, H.; Dornheim, M.; Klassen, T.; Milanese, C.; Gennari, F.; Pistidda, C. Recent Progress and New Perspectives on Metal Amide and Imide Systems for Solid-State Hydrogen Storage. *Energies* **2018**, *11*, 1027.
(6) Chen, P.; Xiong, Z.; Luo, J.; Lin, J.; Tan, K. L. Interaction of Hydrogen with Metal Nitrides and Imides. *Nature* **2002**, *420*, 302−304.
(7) Zhang, T.; Isobe, S.; Matsuo, M.; Orimo, S.-i.; Wang, Y.; Hashimoto, N.; Ohnuki, S. Effect of Lithium Ion Conduction on Hydrogen Desorption of $LiNH_2$−LiH Solid Composite. *ACS Catal.* **2015**, *5*, 1552−1555.
(8) Xiong, Z.; Wu, G.; Hu, J.; Chen, P. Ternary Imides for Hydrogen Storage. *Adv. Mater.* **2004**, *16*, 1522−1525.
(9) Nakamori, Y.; Kitahara, G.; Orimo, S. Synthesis and Dehydriding Studies of Mg−N−H Systems. *J. Power Sources* **2004**, *138*, 309−312.
(10) Zhang, J.; Liu, Y.; Zhang, X.; Yang, Y.; Zhang, Q.; Jin, T.; Wang, Y.; Gao, M.; Sun, L.; Pan, H. Synthesis of CsH and Its Effect on the Hydrogen Sstorage Properties of the $Mg(NH_2)_2$-2LiH System. *Int. J. Hydrogen Energy* **2016**, *41*, 11264−11274.
(11) Luo, W. ($LiNH_2$−MgH_2): a Viable Hydrogen Storage System. *J. Alloys Compd.* **2004**, *381*, 284−287.
(12) Nakamori, Y.; Kitahara, G.; Miwa, K.; Ohba, N.; Noritake, T.; Towata, S.; Orimo, S. Hydrogen Storage Properties of Li−Mg−N−H Systems. *J. Alloys Compd.* **2005**, *404*−*406*, 396−398.
(13) Ichikawa, T.; Hanada, N.; Isobe, S.; Leng, H. Y.; Fujii, H. Hydrogen Storage Properties in Ti Catalyzed Li−N−H system. *J. Alloys Compd.* **2005**, *404*−*406*, 435−438.
(14) Hu, J.; Wu, G.; Liu, Y.; Xiong, Z.; Chen, P.; Murata, K.; Sakata, K.; Wolf, G. Hydrogen Release from Mg(NH2)2−MgH2 through Mechanochemical Reaction. *J. Phys. Chem. B* **2006**, *110*, 14688−14692.
(15) Cao, H.; Zhang, Y.; Wang, J.; Xiong, Z.; Wu, G.; Chen, P. Materials Design and Modification on Amide-based Composites for Hydrogen Storage. *Prog. Nat. Sci.: Mater. Int.* **2012**, *22*, 550−560.
(16) Chen, P.; Xiong, Z.; Wu, G.; Liu, Y.; Hu, J.; Luo, W. Metal−N−H Systems for the Hydrogen Storage. *Scr. Mater.* **2007**, *56*, 817−822.
(17) Jain, A.; Miyaoka, H.; Ichikawa, T. Two-Peak Mystery of $LiNH_2$−NaH Dehydrogenation Is Solved? A Study of the Analogous Sodium Amide/Lithium Hydride System. *J. Phys. Chem. C* **2016**, *120*, 27903−27909.
(18) Ley, M. B.; Jepsen, L. H.; Lee, Y.-S.; Cho, Y. W.; Bellosta von Colbe, J. M.; Dornheim, M.; Rokni, M.; Jensen, J. O.; Sloth, M.; Filinchuk, Y.; et al. Complex Hydrides for Hydrogen Storage − New Perspectives. *Mater. Today* **2014**, *17*, 122−128.
(19) Lin, H.-J.; Li, H.-W.; Murakami, H.; Akiba, E. Remarkably Improved Hydrogen Storage Properties of $LiNH_2$-LiH Composite via the Addition of CeF_4. *J. Alloys Compd.* **2018**, *735*, 1017−1022.
(20) Lin, H.-J.; Li, H.-W.; Paik, B.; Wang, J.; Akiba, E. Improvement of Hydrogen Storage Property of Three-Component $Mg(NH_2)_2$-$LiNH_2$-LiH Composites by Additives. *Dalton Trans.* **2016**, *45*, 15374−15381.
(21) Ichikawa, T.; Hanada, N.; Isobe, S.; Leng, H.; Fujii, H. Mechanism of Novel Reaction from $LiNH_2$ and LiH to Li_2NH and H_2 as a Promising Hydrogen Storage System. *J. Phys. Chem. B* **2004**, *108*, 7887−7892.
(22) Leng, H.; Ichikawa, T.; Hino, S.; Nakagawa, T.; Fujii. Mechanism of Hydrogenation Reaction in the Li−Mg−N−H System. *J. Phys. Chem. B* **2005**, *109*, 10744−10748.
(23) David, W. I. F.; Makepeace, J. W.; Callear, S. K.; Hunter, H. M. A.; Taylor, J. D.; Wood, T. J.; Jones, M. O. Hydrogen Production from Ammonia Using Sodium Amide. *J. Am. Chem. Soc.* **2014**, *136*, 13082−13085.
(24) Makepeace, J. W.; Wood, T. J.; Hunter, H. M. A.; Jones, M. O.; David, W. I. F. Ammonia Decomposition Catalysis Using Non-stoichiometric Lithium Imide. *Chem. Sci.* **2015**, *6*, 3805−3815.
(25) Guo, J.; Wang, P.; Wu, G.; Wu, A.; Hu, D.; Xiong, Z.; Wang, J.; Yu, P.; Chang, F.; Chen, Z.; et al. Lithium Imide Synergy with 3d Transition-Metal Nitrides Leading to Unprecedented Catalytic Activities for Ammonia Decomposition. *Angew. Chem., Int. Ed.* **2015**, *54*, 2950−2954.
(26) Wang, P.; Chang, F.; Gao, W.; Guo, J.; Wu, G.; He, T.; Chen, P. Breaking Scaling Relations to Achieve Low-temperature Ammonia Synthesis Through LiH-mediated Nitrogen Transfer and Hydrogenation. *Nat. Chem.* **2017**, *9*, 64−70.
(27) Leng, H. Y.; Ichikawa, T.; Hino, S.; Hanada, N.; Isobe, S.; Fujii, H. New Metal−N−H System Composed of $Mg(NH_2)_2$ and LiH for Hydrogen Storage. *J. Phys. Chem. B* **2004**, *108*, 8763−8765.
(28) Song, Y.; Yang, R. Decomposition Mechanism of Magnesium Amide $Mg(NH_2)_2$. *Int. J. Hydrogen Energy* **2009**, *34*, 3778−3783.
(29) Cao, H.; Guo, J.; Chang, F.; Pistidda, C.; Zhou, W.; Zhang, X.; Santoru, A.; Wu, H.; Schell, N.; Niewa, R.; et al. Transition and Alkali Metal Complex Ternary Amides for Ammonia Synthesis and Decomposition. *Chem.—Eur. J.* **2017**, *23*, 9766−9771.
(30) Kresse, G.; Hafner, J. Ab Initio Molecular Dynamics for Liquid Metals. *Phys. Rev. B: Condens. Matter Mater. Phys.* **1993**, *47*, 558−561.
(31) Kresse, G.; Furthmüller, J. Efficiency of Ab-Initio Total Energy Calculations for Metals and Semiconductors Using a Plane-Wave Basis Set. *Comput. Mater. Sci.* **1996**, *6*, 15−50.
(32) Kresse, G.; Furthmüller, J. Efficient Iterative Schemes for *Ab Initio* Total-Energy Calculations Using a Plane-Wave Basis Set. *Phys. Rev. B: Condens. Matter Mater. Phys.* **1996**, *54*, 11169−11186.
(33) Perdew, J. P.; Burke, K.; Ernzerhof, M. Generalized Gradient Approximation Made Simple. *Phys. Rev. Lett.* **1996**, *77*, 3865−3868.
(34) Kresse, G.; Joubert, D. From Ultrasoft Pseudopotentials to the Projector Augmented-Wave Method. *Phys. Rev. B: Condens. Matter Mater. Phys.* **1999**, *59*, 1758−1775.
(35) Monkhorst, H. J.; Pack, J. D. Special Points for Brillouin-Zone Integrations. *Phys. Rev. B: Solid State* **1976**, *13*, 5188−5192.

DOI: 10.1021/acs.jpcc.9b03524
J. Phys. Chem. C 2019, 123, 18180−18186

(36) Song, Y.; Guo, Z. X. Electronic Structure, Stability and Bonding of the Li-N-H Hydrogen Storage System. *Phys. Rev. B: Condens. Matter Mater. Phys.* **2006**, *74*, 195120.
(37) Chen, X.; Li, R.; Xia, G.; He, H.; Zhang, X.; Zou, W.; Yu, X. First-principles Study of Decomposition Mechanisms of $Mg(BH_4)_2 \cdot 2NH_3$ and $LiMg(BH_4)_3 \cdot 2NH_3$. *RSC Adv.* **2017**, *7*, 31027−31032.
(38) German, E.; Gebauer, R. Hydrogen Divacancy Diffusion: a New Perspective on H Migration in MgH_2 Materials for Energy Storage. *Phys. Chem. Chem. Phys.* **2017**, *19*, 1174−1180.
(39) Tang, J.-J.; Yang, X.-B.; OuYang, L.; Zhu, M.; Zhao, Y.-J. A Systematic First-principles Study of Surface Energies, Surface Relaxation and Friedel Oscillation of Magnesium Surfaces. *J. Phys. D: Appl. Phys.* **2014**, *47*, 115305.
(40) Ouyang, L.; Tang, J.; Zhao, Y.; Wang, H.; Yao, X.; Liu, J.; Zou, J.; Zhu, M. Express Penetration of Hydrogen on Mg(10$\bar{1}$3) Along the Close-packed-planes. *Sci. Rep.* **2015**, *5*, 10776.
(41) Tang, J.-J.; Yang, X.-B.; Chen, L.-J.; Zhao, Y.-J. Modeling and Stabilities of Mg/MgH_2 Interfaces: A First-principles Investigation. *AIP Adv.* **2014**, *4*, 077101.
(42) Lin, H.-J.; Tang, J.-J.; Yu, Q.; Wang, H.; Ouyang, L.-Z.; Zhao, Y.-J.; Liu, J.-W.; Wang, W.-H.; Zhu, M. Symbiotic $CeH_{2.73}/CeO_2$ Catalyst: A Novel Hydrogen Pump. *Nano Energy* **2014**, *9*, 80−87.
(43) Sørby, M. H.; Nakamura, Y.; Brinks, H. W.; Ichikawa, T.; Hino, S.; Fujii, H.; Hauback, B. C. The Crystal Structure of $LiND_2$ and $Mg(ND_2)_2$. *J. Alloys Compd.* **2007**, *428*, 297−301.
(44) Seip, T. A. T.; Olsen, R. A.; Løvvik, O. M. Surfaces and Clusters of $Mg(NH_2)_2$ Studied by Density Functional Theory Calculations. *J. Phys. Chem. C* **2009**, *113*, 21648−21656.
(45) David, W. I. F.; Jones, M. O.; Gregory, D. H.; Jewell, C. M.; Johnson, S. R.; Walton, A.; Edwards, P. P. A Mechanism for Non-stoichiometry in the Lithium Amide/Lithium Imide Hydrogen Storage Reaction. *J. Am. Chem. Soc.* **2007**, *129*, 1594−1601.
(46) Yang, J. B.; Zhou, X. D.; Cai, Q.; James, W. J.; Yelon, W. B. Crystal and Electronic Structures of $LiNH_2$. *Appl. Phys. Lett.* **2006**, *88*, 041914.
(47) Nagib, M.; Kistrup, H.; Jacobs, H. Neutronenbeugung am Natriumdeuteroamid. NaND2. *Atomkernenergie* **1975**, *26*, 87−90.
(48) Zhong, Y.; Zhou, H.-Y.; Hu, C.-H.; Wang, D.-H.; Oganov, A. R. Theoretical Studies of High-Pressure Phases, Electronic Structure, and Vibrational Properties of $NaNH_2$. *J. Phys. Chem. C* **2012**, *116*, 8387−8393.
(49) Yao, J. H.; Shang, C.; Aguey-Zinsou, K. F.; Guo, Z. X. Desorption Characteristics of Mechanically and Chemically Modified $LiNH_2$ and ($LiNH_2$+LiH). *J. Alloys Compd.* **2007**, *432*, 277−282.

DOI: 10.1021/acs.jpcc.9b03524
J. Phys. Chem. C 2019, 123, 18180−18186